An Updated Performance Metric for Preference-Based Evolutionary Multi-Objective Optimization Algorithms

Deepanshu Yadav
Indian Institute of Technology Madras
Chennai, Tamil Nadu, India
deepanshu.yadav380@gmail.com

Palaniappan Ramu
Indian Institute of Technology Madras
Chennai, Tamil Nadu, India
palramu@iitm.ac.in

Kalyanmoy Deb
Michigan State University
East Lansing, Michigan, USA
kdeb@egr.msu.edu

COIN Report Number 2024003

ABSTRACT

Evolutionary multi-objective optimization (EMO) algorithms are widely used to solve problems involving multiple conflicting objectives. In general, these problems result in a well-distributed and diverse set of Pareto-optimal solutions, consisting of individual objective-optimal solutions at their extreme and various compromise objective solutions at their core. However, in practice, decision-makers (DMs) usually have certain pre-conceived preference information which may make a majority of the Pareto solution set uninteresting to the DMs. In such cases, DM's preference information can be utilized to update EMO algorithms to focus on the preferred part of the Pareto set, rather than the entire Pareto set. While EMO researchers have proposed preference-based EMO algorithms for this purpose, appropriate metrics to evaluate their performance have received lukewarm attention. In this paper, we critically analyze a recently proposed preference-based hypervolume (R-HV) metric for its sensitivity to handle various scenarios and propose an updated version to remedy the difficulties associated with it. The updated R-HV metric is then compared with the original R-HV metric on solutions obtained from a number of preference-based EMO algorithms. The suggestion of a more appropriate R-HV metric presented in this paper should encourage further research in preference-based multi-objective optimization.

CCS CONCEPTS

• **Applied computing → Multi-criterion optimization and decision-making**.

KEYWORDS

Evolutionary Algorithms, Multi-Objective Optimization, Pareto Front, Reference Point, Preference-Based Optimization.

ACM Reference Format:
Deepanshu Yadav, Palaniappan Ramu, and Kalyanmoy Deb. 2024. An Updated Performance Metric for Preference-Based Evolutionary Multi-Objective Optimization Algorithms. In *Genetic and Evolutionary Computation Conference (GECCO '24), July 14–18, 2024, Melbourne, VIC, Australia.* ACM, New York, NY, USA, 9 pages. https://doi.org/10.1145/3638529.3654031

GECCO '24, July 14–18, 2024, Melbourne, VIC, Australia

ACM ISBN 979-8-4007-0494-9/24/07…$15.00
https://doi.org/10.1145/3638529.3654031

1 INTRODUCTION

Many real-world applications consist of multiple and generally conflicting objectives. Such scenarios in literature are classified and formulated as multi-objective optimization (MOO) problems [5, 21]. For solving such problems, evolutionary multi-objective optimization (EMO) algorithms are increasingly being used. These algorithms include NSGA-II [11], MOEA/D [35], RVEA [4], NSGA-III [15], and C-TAEA [17], among others. The task of EMO algorithms is to provide a well-distributed and diverse set of Pareto-optimal (PO) solutions lying on a so-called PO front. One property of the PO front is that an improvement in one objective function can only come at the cost of deteriorating one or more other objective functions [5, 6].

In practice, decision makers (DMs) are not interested in all possible PO solutions. Instead, they seek only a part of PO front satisfying their expert preferences [33]. Though, defining a preference is not an easy task for DMs, preference learning techniques [26–28] provide guidelines for systematic preference elicitation methods to arrive at a specific preferred solution using a plethora of multi-criteria decision-making (MCDM) methods.

Contrary to classical MCDM methods, preference-based evolutionary multi-objective optimization (R-EMO) algorithms find multiple yet non-dominated preferred PO solutions at the region of interest, rather than a single preferred solution. A stand-alone application of R-EMO requires users to have a priori knowledge of the preference information, but instead of finding the entire PO front, R-EMO algorithms focus on a small preferred part of the PO front. Noteworthy techniques for this purpose include R-NSGA-II [12], R-NSGA-III [29], RD-NSGA-II [9], and ROI-NSGA-II [20]. Additionally, Pareto dominance-based evolutionary R-EMO methods such as r-NSGA-II [25], g-NSGA-II [24], and $\hat{g}$-NSGA-II [19] leverage DM preferences expressed as aspiration levels to guide the search towards interesting regions of the PO front using reference point-based EMO algorithms [31]. Light beam search methods presented in [10] and [16] are also encompassed within the R-EMO algorithmic framework. The advantage of the R-EMO approach is its capability to provide focused solutions with faster convergence, especially in higher dimensional problems.

The rise in interest in R-EMO algorithms has emphasized the importance of reliable performance indicators [37]. To assess the efficacy of R-EMO algorithms, several performance metrics have been introduced so far to quantify the convergence and diversity

of R-EMO algorithms. [30] is one of the first attempts in this direction that used the region of interest (RoI) as a hypercube and identified preferred solutions in the RoI. The preferred solutions in the RoI are used to evaluate the hypervolume (HV) metric without considering the preference information of DM. [23] analyzed and highlighted that the method proposed in [30] is sensitive to the relative location of the ideal point and R-EMO solutions affecting the accurate identification of the RoI. [18] demonstrated that the regular HV [36] and IGD [2] metrics are not reliable for evaluating the performance of R-EMO algorithms. Further, the limitation of the metric discussed in [23, 30] are highlighted, and the concept of Achievement Scalarization Function (ASF) [31] is used to propose the reference point-based metric (R-HV and R-IGD). PMOD [14] and Expanding Hypercube metric (EH-metric [1]) are two recently proposed performance indicators for R-EMO. In this study, we first list some limitations of the existing R-HV metric that may introduce a positional bias against certain partial PO sets, specifically for higher objectives. Thereafter, we propose a modified version of R-HV (we call $\widehat{\text{R}}$-HV) to alleviate the limitations.

The rest of the paper is organized as follows. Section 2 provides a detailed discussion based on existing performance indicators for R-EMO algorithms and their limitations considering the R-HV metric. The proposed approach for $\widehat{\text{R}}$-HV computation is presented in Section 3. Simulation results are presented in Section 4 followed by the conclusions in Section 5.

2 EXISTING PERFORMANCE INDICATORS AND THEIR LIMITATIONS

The baseline criteria for the recently proposed performance indicators such as UPCF [23], R-metric [18], PMOD [14], and EH-metric are provided in [23] and listed as follows: (i) set RoI closer to reference point, (ii) account for both convergence and diversity, (iii) need not require knowledge of PO front, and (iv) must be scalable in higher dimensions. Accordingly, recently proposed R-EMO algorithms attempted to account for the above baseline criteria. However, in practice, R-EMO solutions can have an offset or positional bias from the reference line (refer to solutions in Figure 1), indicating a lacuna with the algorithm. Hence, it is important to accommodate this positional bias by the performance indicators, appropriately. Specifically, if the level of offset for two sets of R-EMO solutions from a reference line is the same, their performance indicator must also be the same. The few existing approaches [23, 30] and other metrics, such as R-HV, PMOD, and EH-metric, did not account for the impact of offset R-EMO solutions while deriving the performance indicators. In addition, the existing performance indicators may not always produce better metric values for a set dominating another set.

2.1 R-HV Metric

The R-HV metric for evaluating R-EMO algorithms was designed by borrowing a well-known MCDM concept [18]. In Figure 1, R is the user-defined reference point and O is the ideal point. Assume that three different R-EMO sets are to be compared, as illustrated in Figure 1. DM defines the region of interest (RoI) and solutions falling outside RoI are discarded for R-HV computation. Next, the filtered solution inside the RoI is used to compute the centroid

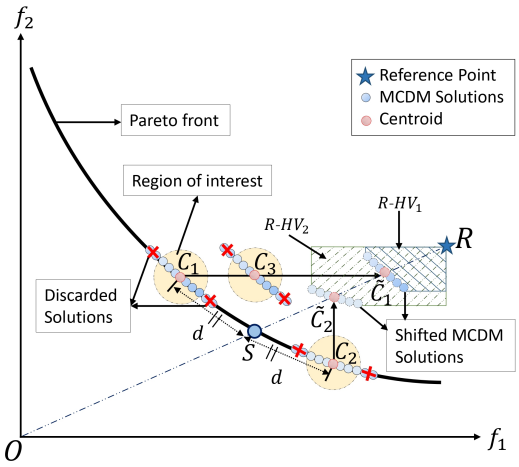

Figure 1: Existing approach for R-HV computation.

C_1, C_2, and C_3. In the next step, each centroid is translated on the reference line using the concept of achievement scalarization function (ASF) (along iso-ASF lines) to obtain a new centroid $\widetilde{C}_1$ or $\widetilde{C}_2$ or $\widetilde{C}_1$, respectively. In the two-objective (f_1 and f_2) case, it is easy to infer that depending upon the location of the centroid with respect to the reference line RO, the centroid is shifted horizontally or vertically.

In the final step, all R-EMO solutions are shifted along the direction of the line joining their centroid (C_1, C_2, and C_3) and respectively shifted centroid ($\widetilde{C}_1$, $\widetilde{C}_2$, and $\widetilde{C}_1$) on reference line RO. Then, these shifted/translated solutions are used for the HV computation from a pre-defined worst point R. The area depicted by the solid hatch lines and dashed hatched lines denote the R-HV$_1$ and R-HV$_2$, respectively. Hence, solutions corresponding to the centroid C_1, C_2, and C_3 has R-HV metric of R-HV$_1$, R-HV$_2$, and R-HV$_1$, respectively.

2.2 Requirements of an Ideal Performance Metric

Results from R-EMO run can appear anywhere near the ideal preferred point (IPP) on the PO front (S). An ideal performance metric must evaluate R-EMO set, properly so that certain obvious facts are honored by the metric [37]. In all criteria mentioned below, the distance from IPP to a set is computed as the normalized Euclidean distance of the centroid of the set from IPP in the objective space. We mention them in the following with respect to three sets of hypothetical R-EMO solutions shown in Figure 1.

(1) **Closeness criterion:** The closer the set is to IPP (S), the better the performance of the R-EMO algorithm. Hence, the metric value should reduce as the set goes away from S in all directions along the PO front. Notice that in the absence of set C_1, the set having centroid at C_3 should have a higher metric value than the set having centroid at C_2, due to the former being closer to IPP, satisfying the closeness criterion.
(2) **Identical distance criterion:** If two non-dominated sets are equidistant from the IPP, they should be assigned identical metric values. In the example sets in the figure, sets with centroid at C_1 and at C_2 should have identical metric values.

(3) **Domination criterion:** If one set is dominated by another set, metric value of the former set should be smaller than that of the latter. In Figure 1, sets with centroid at C_1 should have a larger metric value than that at C_3.
(4) **Spread criterion:** Bounded by RoI, a set having a smaller spread must have a smaller metric value. In the figure, all sets were found wider than RoI, hence after trimming, all three sets have the same spread. But, if we imagine C_1 having a smaller spread than C_2, then despite them being equidistant from IPP, C_1 set should have a smaller metric value, indicating a penalty being assigned to the algorithm for not finding a desired spread of R-EMO solutions.

2.3 Limitations of R-HV

In the following, we investigate how the existing R-HV metric [18] would satisfy the above ideal criteria. According to the R-HV values (area) shown in Figure 1, it is clear that

(1) R-HV(C_3) < R-HV(C_2), thereby violating the closeness criterion.
(2) R-HV(C_1) < R-HV(C_2), thereby violating the identical distance criterion.
(3) R-HV(C_1) = R-HV(C_3), thereby violating the domination criterion.
(4) Spread condition cannot be evaluated from the three example sets, as they have identical spread within their RoIs.

The use of ASF metric in R-HV causes weak PO solutions [21] to have identical values.

R-HV seems to violate the first three criteria in this illustration. We argue that the extent of violation of the closeness and identity criteria will be more prevalent in higher dimensions. In general, R-HV should honor the spread condition (more spread providing more hypervolume value), but the violation of other criteria may offset the actual metric value and cause a violation of the overall desired outcome.

Another limitation of the R-HV metric is worth mentioning. Let us assume that the set C_3 is located on the reference line SR, but a bit above the IPP, meaning that IPP dominates the revised centroid C_3, but C_1 and C_3 are non-dominated to each other. In this case, R-HV(C_3) will be higher than R-HV(C_1), satisfying the closeness criterion. However, the fact that the set C_1 lies on the true PO front and the revised set C_3 is not, makes no effect on R-HV. It is assumed that domination checks are made only with respect to obtained R-EMO sets and they have no underpinnings on whether one set is closer to the true PO front or not. This raises a fifth criterion (**convergence criterion**), that most performance metrics used in EMO algorithms do not use, except a few, such as GD, IGD, and IGD+. Although identifying a set being close to the true PO front requires knowledge of the true PO front, at the least, it demands that a few PO points (such as IPP and other projected PO points) need to be found with additional evaluations. Only with these extra evaluations, we would be able to come up with a true performance of an R-EMO in not only comparing its domination level with another set, its spread, and its location from IPP, but also importantly it can compare and quantify the closeness of solutions to the true PO front, near or away from IPP. We include this as the fifth criterion which a performance metric should have.

3 PROPOSED APPROACH FOR UPDATED R-HV ($\widehat{\text{R}}$-HV) COMPUTATION

We consider all five criteria to define our updated R-HV ($\widehat{\text{R}}$-HV) metric. By introducing Uniform Shift Procedure and Domination Factor, we propose an updated R-HV ($\widehat{\text{R}}$-HV) that satisfies all five aforementioned criteria. The pseudo-code to compute updated metric ($\widehat{\text{R}}$-HV) is presented in Algorithm 1. Assume that given a reference point

Algorithm 1: Updated R-HV ($\widehat{\text{R}}$-HV) Computation

Data: Reference point (R), Ideal Point (O), RoI (δ), Preferred Solutions ($\mathcal{S}$)
Result: Updated R-HV metric ($\widehat{\text{R}}$-HV) for $\mathcal{S}$

```
for i ← 1 to k do
    Č_i ← (1/|S|) Σ_{j=1}^{|S|} f_i[S_j]; // Compute mean of S
C ← S ∈ {S_j | argmin_{j=1}^{|S|} dist(Č, S_j)}; // Centroid of S
for j ← 1 to |S| do
    S_f ← S ∈ {S(j) | dist(S(j), C) ≤ δ}; // Filtering preferred solutions in RoI
Compute R̃-HV using Algorithm 2; // Uniform Shift
Compute the d_f using Algorithm 3; // Domination Factor
R̂-HV ← d_f × R̃-HV; // Updated R-HV Metric
```

R (Figure 2), an R-EMO algorithm is used to compute a solution set. Next, all solutions within RoI (δ-neighbor) of the set are filtered.

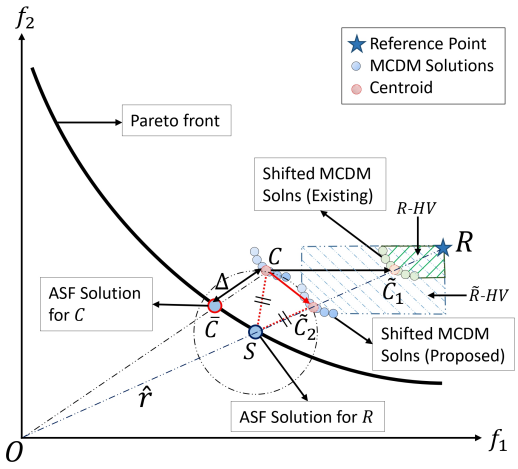

Figure 2: Proposed updated R-HV approach.

The centroid of the filtered solutions is presented by C in Figure 2. The Uniform Shift Procedure (USP), described in Algorithm 2, is used to shift the centroid and their respective solutions along the direction of $C\widetilde{C_2}$. These shifted solutions are used to compute the apparent R-HV metric ($\widetilde{\text{R}}$-HV). Next the distance $CS = \Delta$ is computed to evaluate Domination Factor (d_f). The pseudo-codes the Domination Factor Computation (DFC) is presented in Algorithm 3.

3.1 Uniform Shift Procedure (USP)

We propose Uniform Shift Procedure (USP) (presented in Figure 2) to ensure satisfaction of the identity criterion. It requires IPP (point S) which is located on the reference line RO. The following augmented version of ASF (AASF) [22] is minimized to compute IPP:

$$s\big(f(\mathbf{x})\big) = \max_{i=1,\ldots,k}\left[\frac{f_i - z_i^{**}}{\bar{z}_i - z_i^{**}}\right] + \rho\sum_{i=1}^{k}\left[\frac{f_i}{\bar{z}_i - z_i^{**}}\right], \tag{1}$$

where ρ>0 is a sufficiently small ($\approx 10^{-3}$) scalar (augmentation parameter), f_i is the ith objective function, $\mathbf{z}^{**}$ (slightly smaller than ideal point $\mathbf{z}^*$) is Utopian vector, and $\overline{\mathbf{z}}$ is reference point vector. The second term in the scalarization function $s\big(f(\mathbf{x})\big)$ avoids converging to a weakly PO solution and ensures finding a PO solution, thereby eliminating the demonstrated problem with R-HV in Subsection 2.3.

Upon evaluating the IPP (S), the distance between the point S and centroid C of R-EMO solutions is calculated. A point $\widetilde{C}_2$ on reference line RO is obtained such that $CS = C\widetilde{C}_2$. However, the existing procedure for centroid shift gives the point $\widetilde{C}_1$. The preferred solutions shifted using the existing procedure and the proposed USP is presented in Figure 2. The shaded area with blue dashed hatched/inclined lines represents the apparent R-HV denoted as $\widetilde{\text{R}}$-HV. Whereas the shaded area represented with green solid hatched lines represents the original R-HV. It is to be noted that $\widetilde{\text{R}}$-HV is significantly different from the existing R-HV metric. The steps involved in USP are presented in Algorithm 2.

Algorithm 2: Uniform Shift Procedure (USP)

Data: Reference point (R), Ideal Point (O), centroid (C), Filtered solution in RoI ($\mathcal{S}_f$)
Result: Apparent R-HV Metric ($\widetilde{\text{R}}$-HV)

$S \leftarrow$ Solve AASF equation 1; // `Pareto optimal point` S
$CS \leftarrow \text{dist}(C, S)$; // `dist is euclidean distance`
$\widetilde{C}_2 \leftarrow \vec{S} + CS \times \widehat{\text{r}}$; // `Shifting centroid` C `to` $\widetilde{C}_2$, $\widehat{\text{r}}$ `is unit vector along reference vector` $\overrightarrow{OR}$
$\mathcal{S}_f^{'} \leftarrow \mathcal{S}_f + \overrightarrow{C\widetilde{C}_2}$; // `Shifting filtered solutions`
$\widetilde{\text{R}}\text{-HV} \leftarrow \mathcal{H}(\mathcal{S}_f^{'})$; // $\mathcal{H}$ `is hypervolume`

The USP ensures that centroid and other solutions located on a hyper-sphere with center S and radius CS are shifted to a common point $\widetilde{C}_2$ on the reference line RO. It is to be noted that R-EMO solutions, shown in Figure 2, are dominated, hence $\widetilde{\text{R}}$-HV is apparent R-HV metric. To obtain the updated R-HV, Domination Criteria must be taken into account which is discussed in the next section. However, USP ensures the identity criterion for two sets of R-EMO solutions that are Pareto-optimal with their centroid located equidistant from point S.

3.2 Domination Factor Computation (DFC)

To account for the domination criteria, we propose a Domination Factor Computation (DFC) method. In the previous discussion, we emphasized that USP shifts all the centroid (in criterion space) located on the circumference of the hyper-sphere, uniformly (Figure 2). Hence all R-EMO solutions with the centroid lying on the circumference of the hyper-sphere have identical values of apparent R-HV denoted as $\widetilde{\text{R}}$-HV. However, there exist many sets of solutions whose centroid lie on the hyper-sphere but get dominated by a specific set whose centroid is at the intersection of the true PO front and the hyper-sphere. According to the dominance criterion, the latter set should have a higher $\widetilde{\text{R}}$-HV than the former. Thus, we make one modification to $\widetilde{\text{R}}$-HV and multiply it with a Domination Factor (d_f).

Algorithm 3: Domination Factor Computation (DFC)

Data: Ideal point (O), Reference point (R), Centroid (C), IPP (S)
Result: Domination Factor (d_f)

$\bar{C} \leftarrow$ Solve AASF in equation 1; // `Obtain Pareto optimal point` $\bar{C}$
$\Delta \leftarrow \text{dist}(C\bar{C})$; // `Compute distance` Δ
$SR \leftarrow \text{dist}(S, R)$; // `Compute the distance` SR
$d_f \leftarrow$ Solve equation 2; // `Compute Domination Factor`

The computation of d_f is explained as follows. Consider the centroid C in Figure 2 that corresponds to a set of dominated sets. Next, considering C as a reference point vector ($\overline{\mathbf{z}}$), AASF formulation presented in Equation 1 is solved to obtain a true PO point $\bar{C}$. The distance between the points C and $\bar{C}$ (denoted by Δ in the figure) is computed as the measure of domination. It is noteworthy that if Δ is zero, the point C is Pareto-optimal and the updated R-HV must equal to apparent R-HV: ($\widetilde{\text{R}}$-HV). If $\Delta \geq SR$, the updated R-HV should be zero to signify that R-EMO set is not able to find a set that is better than the worst supplied point R. To account for all these conditions, the domination factor (d_f) is derived as follows:

$$d_f = \max\left[\left(1 - \frac{\Delta}{SR}\right), 0\right]. \tag{2}$$

Finally, the updated R-HV ($\widehat{\text{R}}$-HV) is obtained as follows:

$$\widehat{\text{R}}\text{-HV} = d_f \times \widetilde{\text{R}}\text{-HV}. \tag{3}$$

This updated R-HV metric ($\widehat{\text{R}}$-HV) incorporates all five criteria and hence is an improvement to the existing R-HV metric. But it requires additional function evaluations through a single-objective optimization run in finding the IPP (common for evaluating performance metric for multiple R-EMO sets) and $\bar{C}$ using AASF formulation presented in Equation 1 (executed once for each R-EMO set).

4 SIMULATION RESULTS

The updated metric $\widehat{\text{R}}$-HV and existing R-HV metric are used to compare three EAs on 3 benchmarks and 2 real-world engineering examples listed in Table 1. For all the test cases, first, the preferred solutions are computed using R-NSGA-III [29] algorithm. Then the reference vectors that survived in the last generation of R-NSGA-III are supplied to RVEA [4] and C-TAEA [17] algorithms. The parameters for RVEA (penalty parameter α = 2.0, adaptive frequency f_r = 0) are kept constant. The GA parameters i.e. simulated binary crossover: SBX (cross-over probability p_c=1.0 and crossover operator η_c=30) and polynomial mutation: PM (mutation probability

Table 1: Test Case to compare $\widehat{\text{R}}$-HV and R-HV. M and N represent the number of objective functions and design variables, respectively. N_{RP}, N/#RP and Gen represent the number of reference points, population per reference point, and generation, respectively. μ is the shrinkage factor.

Test Case	M	N	R-NSGA-III				AASF	
			N_{RP}	N/#RP	Gen	μ	N	Gen
2-Bar Truss	2	4	2	20	100	0.10	10	50
Fin. Proc.	2	4	2	10	100	0.15	10	50
Benchmark	3	5	4	21	1000	0.10	50	1000
Benchmark	4	5	1	20	1000	0.10	50	1000
Benchmark	8	10	1	36	1000	0.10	50	1000

η_m=30) are kept the same for all examples. R-NSGA-III and AASF parameters used in the simulation are presented in Table 1. In all the examples, R-NSGA-III solutions are used to compute the RoI defined by δ-neighbourhood. Here, it is assumed that all R-NSGA-III solutions lie inside the RoI, and extreme/corner R-EMO solutions lie on the boundary of the RoI. A pseudo-code for computing δ using R-NSGA-III solution is presented in Algorithm 4.

Algorithm 4: Region of Interest (δ) Computation

Data: R-NSGA-III Solutions ($\mathcal{S}^{R3}$)
Result: δ
for $i \leftarrow 1$ **to** k **do**
  $\check{C}_i^{R3} \leftarrow \frac{1}{|\mathcal{S}^{R3}|} \sum_{j=1}^{|\mathcal{S}^{R3}|} f_i[\mathcal{S}_j^{R3}]$; // Mean of R-NSGA-III solutions
$C \leftarrow \mathcal{S}^{R3} \in \{\mathcal{S}_j^{R3} \mid \underset{j=1}{\overset{|\mathcal{S}^{R3}|}{\text{argmin}}} \text{dist}(\check{C}^{R3}, \mathcal{S}_j^{R3})\}$; // Centroid of R-NSGA-III solutions
for $j \leftarrow 1$ **to** $|\mathcal{S}^{R3}|$ **do**
  $\delta \leftarrow \max \text{dist}(\mathcal{S}^{R3}(j), C)$; // Farthest point from the centroid

4.1 4-Bar Truss with Two Objectives

The 4-Bar truss problem [3] is an unconstrained bi-objective problem. It has four design variables. In Figure 3, black color dots represent the PO front. Two reference points R_1 = [0.4, 0.9] and R_2 = [0.9, 0.4], used here, are represented by blue color stars . Considering R_1 and R_2 as reference points, R-EMO solutions (green color dots) are computed using R-NSGA-III, as shown in Figure 3a. The cyan color dots indicate the solution obtained upon shifting R-NSGA-III solutions (green color) using the existing R-HV approach. The red color dots denote the shifted R-EMO solutions as per the updated $\widehat{\text{R}}$-HV approach. The R-NSGA-III and AASF parameters used are mentioned in Table 1. To make a fair comparison of R-NSGA-III, RVEA, and C-TAEA, the reference directions of the populations in the last generation of R-NSGA-III are preserved and supplied as input to RVEA and C-TAEA. The R-EMO solutions (green dots) obtained using RVEA and C-TAEA are presented in Figure 3b and Figure 3c, respectively.

Next, Algorithm 4 is used to compute the RoI (δ) using R-NSGA-III solutions. The region shown in the pink circle is the region of interest (RoI). In Figures 3a, 3b and 3c, the R-NSGA-III, RVEA and C-TAEA solutions filtered inside RoI are shifted using USP and plotted with red markers. The area shown in the green color region shaded with hatched lines denotes to R-HV metric. Whereas, the yellow color area shaded with horizontal lines denotes $\widetilde{\text{R}}$-HV metric. Table 2 lists the number of R-EMO solutions found (N_0), filtered solutions in RoI (N_δ), R-HV, and $\widehat{\text{R}}$-HV metric values.

Corresponding to reference point R_1, for all of the three algorithms, the R-NSGA-III solutions are closer to the true PO front and are also spread near the reference line (R_1O). Hence, the shifted R-NSGA-III solutions using the existing approach and the proposed approach are closer to the original solutions. Therefore, the effect of USP and DFC is not that significant. The R-HV and $\widehat{\text{R}}$-HV metric are very close to each other (see Table 2). R-NSGA-III has the largest R-HV and $\widehat{\text{R}}$-HV values among all the algorithms. RVEA could only find 17 solutions in RoI which reduces its coverage resulting in relatively small values of R-HV and $\widehat{\text{R}}$-HV. R-EMO solutions obtained using C-TAEA are relatively more offset from the reference line (R_1O) resulting in the smallest R-HV and $\widehat{\text{R}}$-HV values.

For reference point R_2, R-EMO solutions from R-NSGA-III, RVEA, and C-TAEA are part of the Pareto front. Hence, the effect of d_f is negligible. However, the level of offset of R-EMO sets from the reference line R_2O is significant in the case of RVEA, followed by C-TAEA, and R-NSGA-III solutions. Therefore, the effect of USP is significant in the case of RVEA solutions resulting in the lowest values of R-HV and $\widehat{\text{R}}$-HV metric. It is noteworthy that the difference between the R-HV and $\widehat{\text{R}}$-HV metric is relatively large for RVEA as compared to R-NSGA-III and C-TAEA (see Table 2). It can be concluded that if the R-EMO solutions are close to the true PO front and are spread uniformly near the reference line, the effect of USP and DFC is negligible resulting R-HV metric having a similar value to $\widehat{\text{R}}$-HV metric.

4.2 Finishing Process Problem

The abrasive flow finishing process [13] is a real-world unconstrained bi-objective problem. Figure 4 demonstrates the comparison of R-HV and $\widetilde{\text{R}}$-HV metrics. In this example, two reference points R_1 = [0.8, 0.3] and R_2 = [0.3, 0.8], plotted in blue color stars, are considered for evaluating solutions from three R-EMO algorithms – R-NSGA-III, RVEA, and C-TAEA. R-NSGA-III solutions are used to compute the value of δ using Algorithm 4. The parameters used for the R-NSGA-III algorithm are presented in Table 1. The reference direction of R-NSGA-III solutions that survived in the last generation is preserved and supplied as input to RVEA and C-TAEA and the respective R-EMO solutions are computed. With δ as the radius and centroid of R-EMO solutions as the center, a circle filled with pink color (in Figure 4) represents the RoI. The green color region hatched with inclined lines represents the R-HV and the yellow color region hatched with horizontal lines represents the $\widetilde{\text{R}}$-HV. Green, cyan, and red color dots represent the R-EMO solutions, shifted R-EMO solutions using the R-HV approach, and shifted R-EMO solution using USP, respectively.

Consider the reference point R_1 first. R-EMO solutions (green dots) obtained using the three algorithms are presented in Figures

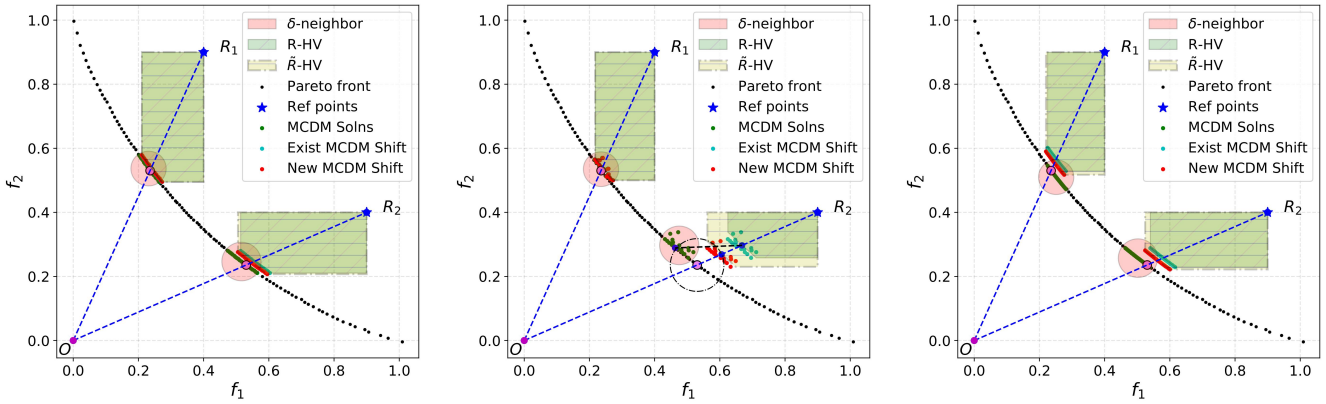

(a) $\widetilde{\text{R}}$-HV computation using R-NSGA-III (b) $\widetilde{\text{R}}$-HV computation using RVEA (c) $\widetilde{\text{R}}$-HV computation using C-TAEA

Figure 3: Demonstration of apparent R-HV metric ($\widetilde{\text{R}}$-HV) on 4-Bar Truss example using R-NSGA-III, RVEA, and C-TAEA. Black color and green color dots represent the non-dominated solutions and R-EMO solutions respectively. Cyan color and red dots represent the shift of R-EMO solutions (green dots) according to existing R-HV and updated R-HV. The region inside the pink circle is the region of interest (RoI). In Sub-figure (b), the black color dashed line and dashed circle demonstrate the concept of shifting R-EMO solution using the existing approach and USP, respectively.

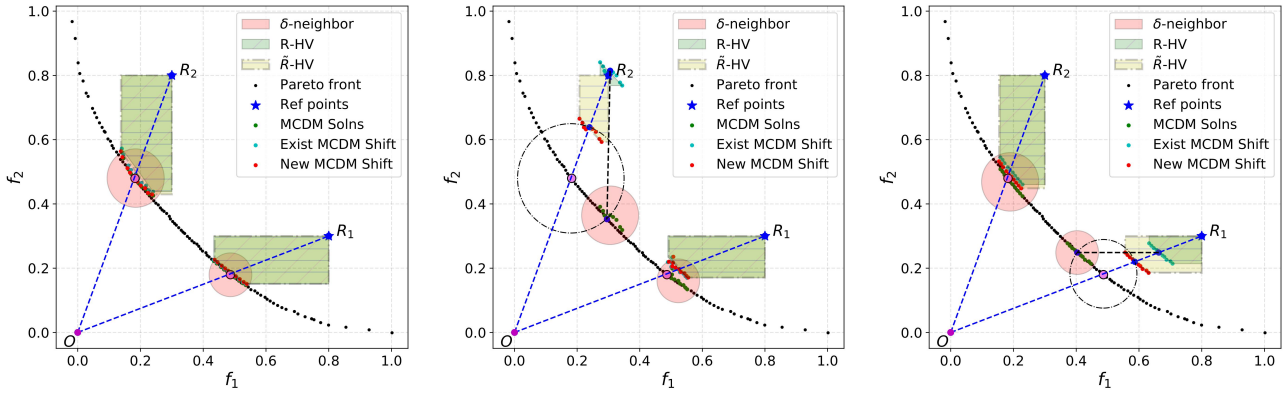

(a) $\widetilde{\text{R}}$-HV computation using R-NSGA-III (b) $\widetilde{\text{R}}$-HV computation using RVEA (c) $\widetilde{\text{R}}$-HV computation using C-TAEA

Figure 4: Comparison of R-HV and $\widetilde{\text{R}}$-HV on Finishing Process example using R-NSGA-III, RVEA, and C-TAEA. R_1 and R_2 are two reference points, O is the ideal point. Black, green, cyan, and red dots represent the Pareto front, R-EMO solution, shifted R-EMO solutions using the existing R-HV approach, and shifted R-EMO using the proposed USP, respectively.

4a, 4b, and 4c. These R-EMO solutions lie on Pareto front causing negligible values of domination factor (d_f). However, the offset of R-EMO solutions from reference line R_1O in C-TAEA is significant followed by RVEA, and is the least in the case of R-NSGA-III solution. Therefore, the impact of USP in C-TAEA is more, followed by RVEA, and is negligible in R-NSGA-III. This results in the smallest value of $\widehat{\text{R}}$-HV metric for C-TAEA solutions. In this case the values of R-HV and $\widehat{\text{R}}$-HV metric presented in Table 2 are governed by the offset of R-EMO solutions from the reference line R_1O. However, it is to be noted that there is a significant difference in R-HV and $\widehat{\text{R}}$-HV metric for C-TAEA solutions.

R-EMO solutions obtained using R-NSGA-III and C-TAEA with the reference point R_2, shown in Figures 4a and 4c, are Pareto optimal. But, RVEA solutions presented in Figure 4b are slightly dominated. Being Pareto-optimal, the effect of DFC is negligible for R-NSGA-III and C-TAEA solutions, but d_f values are relatively larger for RVEA solutions. Moreover, RVEA solutions are largely offset from the reference line R_2O as compared to solutions obtained using the other two R-EMO algorithms. The offset of C-TAEA solutions is relatively small, and that for R-NSGA-III solutions is negligible. Hence, the effect of USP is significant in the case of RVEA solutions, making $\widehat{\text{R}}$-HV small, followed by C-TAEA solutions and R-NSGA-III solutions, in that order. The respective values of R-HV and $\widehat{\text{R}}$-HV metric are presented in Table 2 for clarity. Not surprisingly, the difference in R-HV and $\widehat{\text{R}}$-HV metric for RVEA sets is quite large. These results emphasize the importance of the proposed $\widehat{\text{R}}$-HV as a performance metric for preference-based EMO algorithms, even though the ranks of three R-EMO algorithms provided by both metrics are similar.

The two bi-objective examples discussed compare $\widehat{\text{R}}$-HV with the R-HV metric and demonstrate the effectiveness of the updated

Table 2: Comparison of R-EMO based on R-HV and $\widehat{\text{R}}$-HV metric. N_0 and N_δ denote the number of R-EMO solutions and number of R-EMO solutions in RoI, respectively. The number in bold text indicates that the corresponding R-EMO is the best-performing algorithm for a given reference point.

Test Case	Reference point(s)	Algorithm	N_0	N_δ	R-HV	$\widehat{\text{R}}$-HV
2-Bar Truss	[0.4, 0.9]	R-NSGA-III	20	20	**0.0743**	**0.0740**
		RVEA	17	17	0.0711	0.0707
		C-TAEA	20	20	0.0628	0.0667
	[0.9, 0.4]	R-NSGA-III	20	20	**0.0699**	**0.0729**
		RVEA	19	19	0.0367	0.0530
		C-TAEA	20	20	0.0592	0.0643
Finishing Process	[0.8,0.3]	R-NSGA-III	10	10	**0.0507**	**0.0498**
		RVEA	9	9	0.0387	0.0372
		C-TAEA	10	10	0.0119	0.0254
	[0.3,0.8]	R-NSGA-III	10	10	**0.0519**	**0.0541**
		RVEA	10	10	0.0000	0.0155
		C-TAEA	10	10	0.0448	0.0481
Benchmark (3-Objective)	[0.25, 0.25, 3.0]	R-NSGA-III	21	21	**0.0136**	0.0124
		RVEA	21	15	0.0134	0.0125
		C-TAEA	21	15	0.0049	**0.0155**
	[0.25, 1.0, 3.0]	R-NSGA-III	21	21	**0.0873**	0.0829
		RVEA	21	20	0.0764	0.0715
		C-TAEA	21	18	0.0462	**0.1283**
	[1.0, 0.25, 3.0]	R-NSGA-III	21	21	0.0872	0.0828
		RVEA	21	20	**0.0971**	0.0924
		C-TAEA	21	18	0.0470	**0.1284**
	[1.0, 1.0, 3.0]	R-NSGA-III	21	21	**0.4351**	**0.4252**
		RVEA	21	20	0.3008	0.2800
		C-TAEA	21	21	0.3867	0.4160
Benchmark (4-Objective)	[1.0, 1.0, 1.0, 8.0]	R-NSGA-III	20	20	**1.7978**	1.7205
		RVEA	20	18	0.7743	0.6475
		C-TAEA	20	14	1.1950	**1.8266**
Benchmark (8-Objective)	[1.0, 1.0, 1.0, 1.0, 1.0, 1.0, 1.0, 10.0]	R-NSGA-III	35	35	**0.1201**	**0.2009**
		RVEA	35	33	0.0006	0.0011
		C-TAEA	35	21	0.0090	0.0089

R-HV approach. These two examples are easy to comprehend as the impact of offset of R-EMO solutions from reference lines is visible. In the complex cases where the solutions are offset as well as dominated, and the combined effect is not easy to comprehend, the significance of the proposed updated R-HV is greater, which we will discuss in the upcoming 3- and higher-objective examples.

4.3 Three-objective Benchmark Problem

The benchmark problem mentioned in [8], is considered for three-objective problem. For this example, four reference points – R_1 = [0.25, 0.25, 3.0], R_2 = [0.25, 1.0, 3.00], R_3 = [1.0, 0.25, 3.0], and R_4 = [1.0, 1.0, 3.00] – are considered as user-defined reference points for computing preferred solutions using three R-EMO algorithms – R-NSGA-III, RVEA, and C-TAEA. The reference points, their respective R-EMO solutions, and shifted solutions for $\widehat{\text{R}}$-HV computation are shown in Figure 5. R-EMO solutions for R-NSGA-III, RVEA, and C-TAEA are shown in Figures 5a, 5b and 5c, respectively. We observe that all R-EMO solutions obtained for this problem lie on PO front leading to negligible d_f values. But since all sets are offset from the reference line, $\widehat{\text{R}}$-HV value will be affected. Moreover, the spread of R-EMO solutions in RoI is not identical. These two combined effects make it difficult to make an easy inference of the relative performance of R-EMO algorithms, but $\widehat{\text{R}}$-HV values, along with the number of R-EMO solutions (N_0), number of filtered R-EMO solutions in RoI (N_δ) and original R-HV values are provided in Table 2 for a closer inspection.

For the reference point R_1, R-HV metric suggests that R-NSGA-III performs the best among the three R-EMO algorithms followed by RVEA. C-TAEA has significantly low performance. However, according to the $\widehat{\text{R}}$-HV, C-TAEA has the best performance followed by RVEA, and R-NSGA-III performance is marginally less than RVEA. This opposite trend in R-HV and $\widehat{\text{R}}$-HV metrics requires an explanation and leads to a further justification in favor of using $\widehat{\text{R}}$-HV. Let us concentrate on the shifted solutions obtained by applying USP in Figures 5a and 5c. As RoI is defined by R-NSGA-III solutions, the solutions obtained after USP (Figure 5a) are scattered in a triangular shape. Whereas, due to relatively more coverage of C-TAEA solutions, few solutions are eliminated and the number of solutions in RoI is reduced from 21 to 15. However, these filtered solutions in RoI are arranged in a trapezoidal shape (Figure 5c) that has a bigger area (better coverage) than the triangle in the case of R-NSGA-III. Adding to that, the effect of USP is relatively less in the case of C-TAEA solutions, as compared to the R-NSGA-III and RVEA. Because of these two combined effects, $\widehat{\text{R}}$-HV values are the highest for C-TAEA. However, the shift procedure in the existing R-HV approach shifted the C-TAEA solution shown in yellow color dots in Figure 5c, closer to the reference point. This inappropriate shifting of C-TAEA solutions causes an unusually low value of R-HV, as compared to the other two R-EMO algorithms.

Considering the reference point R_2, the performance of R-NSGA-III is best followed by RVEA according to the R-HV metric. However, according to $\widehat{\text{R}}$-HV metric, C-TAEA has the best performance followed by R-NSGA-III. The reason behind this is the effect of R-EMO shift on the reference line (R_2O) using the existing R-HV procedure and proposed USP. It can be observed from Figure 5, that USP shifts the C-TAEA solutions closer to the Pareto front as compared to R-NSGA-III and RVEA. However, the existing R-HV procedure shifts the C-TAEA solutions far from Pareto front and closer to reference point R_2 in Figure 5c. This results in lower values of R-HV metric and higher values of $\widehat{\text{R}}$-HV metric for C-TAEA solutions. For reference point R_3, RVEA is the best-performing R-EMO algorithm followed by R-NSGA-III considering R-HV metric. But, $\widehat{\text{R}}$-HV metric has the opposite trend because of the significant impact of USP in shifting the R-EMO solutions on reference line R_3. The trend of R-HV and $\widehat{\text{R}}$-HV on three R-EMO is similar for reference point R_4.

4.4 Many-objective Problems

Three objective test cases discussed in [8] are scaled to formulate a 4-objective and an 8-objective test case to demonstrate the performance of R-NSGA-III, RVEA, and C-TAEA algorithms. The algorithmic details and performance measures of R-EMO for these examples are provided in Table1. Figure 6 depicts PCP plots of the PO front, reference point, R-EMO solutions obtained by R-EMO algorithms, and shifted solution using R-HV approach and $\widehat{\text{R}}$-HV approach. The green color lines in Figure 6b being outside the gray region indicates that RVEA solutions are dominated. Hence, for RVEA the Domination factor (d_f) has a vital role in computing $\widehat{\text{R}}$-HV metric. In the case of C-TAEA the R-EMO solutions are part of Pareto front, hence d_f has negligible impact on $\widehat{\text{R}}$-HV computation.

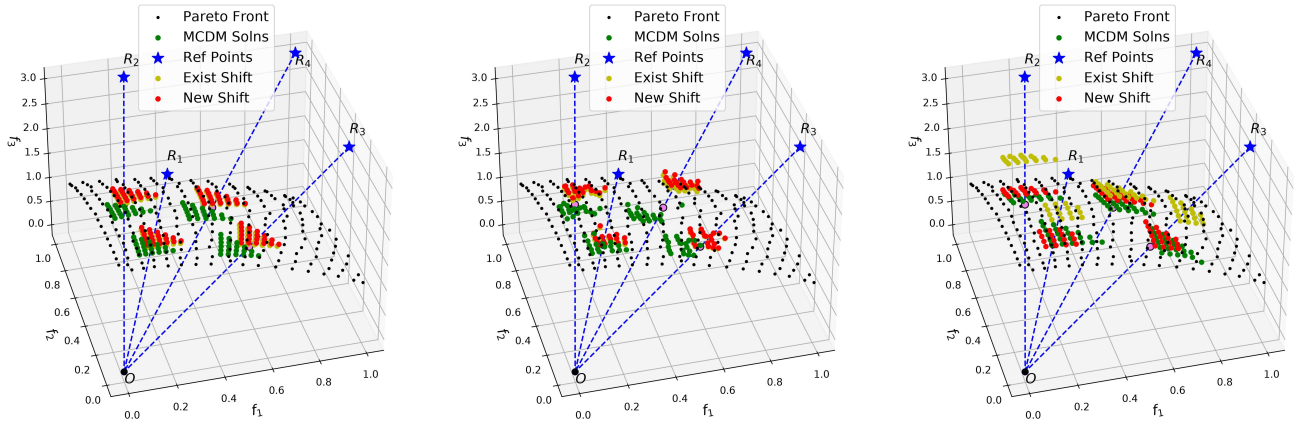

(a) R-EMO solutions obtained using R-NSGA-III **(b) R-EMO solutions obtained using RVEA** **(c) R-EMO solutions obtained using C-TAEA**

Figure 5: Scatter plot for R-EMO solutions obtained by three algorithms and their shifted R-EMO solution on reference line using existing R-HV approach and proposed USP approach on a 3-objective benchmark example. Black, green, yellow, and red color dots represent Pareto front, preferred solutions, shifted R-EMO solution using the existing approach, and shifted R-EMO solutions using the proposed USP approach, respectively. R_1, R_2, R_3, and R_4 denotes the reference points.

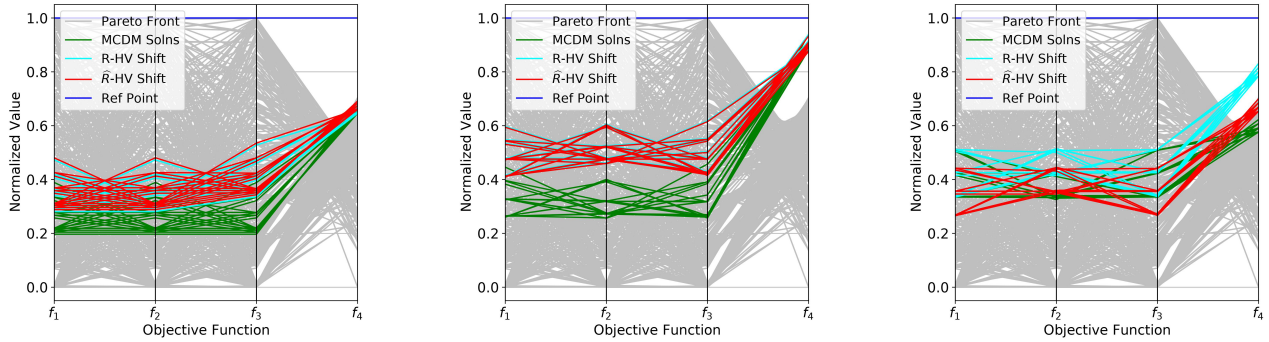

(a) R-EMO solutions obtained using R-NSGA-III **(b) R-EMO solutions obtained using RVEA** **(c) R-EMO solutions obtained using C-TAEA**

Figure 6: PCP plots for R-EMO solutions obtained from R-EMO algorithms and their shifted R-EMO solution on reference line using existing R-HV approach and proposed USP approach on 4-objective benchmark problem.

As the distance between the reference point and R-EMO solutions obtained from RVEA is relatively low (Δ is high) as compared to that of R-NSGA-III and C-TAEA, hence R-HV and $\widehat{\text{R}}$-HV metric is lowest for RVEA. The cyan color and red color lines in Figure 6a are very close so their R-HV and $\widehat{\text{R}}$-HV values are also close. On the contrary, the cyan color lines in Figure 6c are far from red color lines and shifted towards the reference point, therefore, $\widehat{\text{R}}$-HV metric is better than R-HV for C-TAEA. The red lines corresponding to f_1 to f_3 in Figure 6c are far from reference lines as compared to the red lines in 6a, and that in f_4 they are positioned at around similar location. This leads to the better $\widehat{\text{R}}$-HV metric for C-TAEA than R-NSGA-III.

For 8-objective example, R =[1.0, 1.0, 1.0, 1.0, 1.0, 1.0, 1.0, 10.0] is selected as reference point and R-EMO solutions using R-NSGA-III, RVEA, and C-TAEA are computed. The performance measures in terms of N_0, N_δ, R-HV, and $\widehat{\text{R}}$-HV are presented in Table 2. In this case, both the R-HV and $\widehat{\text{R}}$-HV suggest that R-NSGA-III has the best performance, followed by C-TAEA.

5 CONCLUSIONS

This paper has proposed five requirements that a performance metric for truly evaluating R-EMO algorithms must possess. Based on these criteria an existing metric (R-HV) has been criticized and modified to suggest an updated metric ($\widehat{\text{R}}$-HV). The proposed $\widehat{\text{R}}$-HV metric is compared with R-HV metric on three R-EMO algorithms – R-NSGA-III, RVEA, and C-TAEA – considering five test cases with 2- to 8-objective problems. These examples highlight the effectiveness of $\widehat{\text{R}}$-HV metric, such as the effect of dominated R-EMO solutions, the effect of R-EMO solution being offset from the reference line, and the spread of R-EMO solutions in RoI. Also, the combined effect of these scenarios has been presented to highlight the significance of the proposed $\widehat{\text{R}}$-HV metric over the existing R-HV metric.

Though $\widehat{\text{R}}$-HV metric provides a better comparison of R-EMO algorithms than R-HV, it comes at the cost of solving the AASF problem presented in Equation 1. In the future, KKT proximity measure [7] can be used to replace the domination factor for the $\widehat{\text{R}}$-HV computation to achieve a more theoretically accurate measure. The

proposed updated metric ($\widehat{\text{R}}$-HV) can also be extended to evaluate other R-EMO algorithms [9, 12, 24, 25]. $\widehat{\text{R}}$-HV can be used to compare the performance of robust solution-seeking R-EMO algorithms [32, 34] as well. In the future, the computational complexity and efficacy of the proposed $\widehat{\text{R}}$-HV can be statistically compared with recently proposed metrics [1, 14].

REFERENCES

[1] Sunith Bandaru and Henrik Smedberg. 2019. A parameterless performance metric for reference-point based multi-objective evolutionary algorithms. In *Proceedings of the Genetic and Evolutionary Computation Conference*. 499–506.

[2] Peter AN Bosman and Dirk Thierens. 2003. The balance between proximity and diversity in multiobjective evolutionary algorithms. *IEEE transactions on evolutionary computation* 7, 2 (2003), 174–188.

[3] FY Cheng and XS Li. 1999. Generalized center method for multiobjective engineering optimization. *Engineering Optimization* 31, 5 (1999), 641–661.

[4] Ran Cheng, Yaochu Jin, Markus Olhofer, and Bernhard Sendhoff. 2016. A reference vector guided evolutionary algorithm for many-objective optimization. *IEEE Transactions on Evolutionary Computation* 20, 5 (2016), 773–791.

[5] Carlos A Coello Coello, Gary B Lamont, and David A Van Veldhuizen. 2007. *Evolutionary algorithms for solving multi-objective problems*. Vol. 5. Springer.

[6] Kalyanmoy Deb. 2011. Multi-objective optimisation using evolutionary algorithms: an introduction. In *Multi-objective evolutionary optimisation for product design and manufacturing*. Springer, 3–34.

[7] Kalyanmoy Deb, Mohamed Abouhawwash, and Haitham Seada. 2017. A computationally fast convergence measure and implementation for single-, multiple-, and many-objective optimization. *IEEE Transactions on Emerging Topics in Computational Intelligence* 1, 4 (2017), 280–293.

[8] Kalyanmoy Deb and Himanshu Gupta. 2005. Searching for robust Pareto-optimal solutions in multi-objective optimization. In *International conference on evolutionary multi-criterion optimization*. Springer, 150–164.

[9] Kalyanmoy Deb and Abhishek Kumar. 2007. Interactive evolutionary multi-objective optimization and decision-making using reference direction method. In *Proceedings of the 9th annual conference on Genetic and evolutionary computation*. 781–788.

[10] Kalyanmoy Deb and Abhay Kumar. 2007. Light beam search based multi-objective optimization using evolutionary algorithms. In *2007 IEEE Congress on Evolutionary Computation*. IEEE, 2125–2132.

[11] Kalyanmoy Deb, Amrit Pratap, Sameer Agarwal, and Tanaka Meyarivan. 2002. A fast and elitist multiobjective genetic algorithm: NSGA-II. *IEEE transactions on evolutionary computation* 6, 2 (2002), 182–197.

[12] Kalyanmoy Deb and J Sundar. 2006. Reference point based multi-objective optimization using evolutionary algorithms. In *Proceedings of the 8th annual conference on Genetic and evolutionary computation*. 635–642.

[13] Pushpendra Gupta, Vidyapati Kumar, Dilip Kumar Pratihar, and Kalyanmoy Deb. 2023. Multi-objective Optimization of Rotational Magnetorheological Abrasive Flow Finishing Process. (2023).

[14] Zhanglu Hou, Shengxiang Yang, Juan Zou, Jinhua Zheng, Guo Yu, and Gan Ruan. 2018. A performance indicator for reference-point-based multiobjective evolutionary optimization. In *2018 IEEE Symposium Series on Computational Intelligence (SSCI)*. IEEE, 1571–1578.

[15] Himanshu Jain and Kalyanmoy Deb. 2013. An evolutionary many-objective optimization algorithm using reference-point based nondominated sorting approach, part II: Handling constraints and extending to an adaptive approach. *IEEE Transactions on evolutionary computation* 18, 4 (2013), 602–622.

[16] Andrzej Jaszkiewicz and Roman Słowiński. 1999. The 'Light Beam Search' approach–an overview of methodology applications. *European Journal of Operational Research* 113, 2 (1999), 300–314.

[17] Ke Li, Renzhi Chen, Guangtao Fu, and Xin Yao. 2018. Two-archive evolutionary algorithm for constrained multiobjective optimization. *IEEE Transactions on Evolutionary Computation* 23, 2 (2018), 303–315.

[18] Ke Li, Kalyanmoy Deb, and Xin Yao. 2017. R-metric: Evaluating the performance of preference-based evolutionary multiobjective optimization using reference points. *IEEE Transactions on Evolutionary Computation* 22, 6 (2017), 821–835.

[19] Wenjian Luo, Luming Shi, Xin Lin, and Carlos A Coello Coello. 2019. The g-dominance relation for preference-based evolutionary multi-objective optimization. In *2019 IEEE Congress on Evolutionary Computation (CEC)*. IEEE, 2418–2425.

[20] Manu Manuel, Benjamin Hien, Simon Conrady, Arne Kreddig, Nguyen Anh Vu Doan, and Walter Stechele. 2022. Region of interest based non-dominated sorting genetic algorithm-II: an invite and conquer approach. In *Proceedings of the Genetic and Evolutionary Computation Conference*. 556–564.

[21] Kaisa Miettinen. 2012. *Nonlinear multiobjective optimization*. Vol. 12. Springer Science & Business Media.

[22] Kaisa Miettinen and Marko M Mäkelä. 2002. On scalarizing functions in multiobjective optimization. *OR spectrum* 24 (2002), 193–213.

[23] Asad Mohammadi, Mohammad Nabi Omidvar, and Xiaodong Li. 2013. A new performance metric for user-preference based multi-objective evolutionary algorithms. In *2013 IEEE congress on evolutionary computation*. IEEE, 2825–2832.

[24] Julián Molina, Luis V Santana, Alfredo G Hernández-Díaz, Carlos A Coello Coello, and Rafael Caballero. 2009. g-dominance: Reference point based dominance for multiobjective metaheuristics. *European Journal of Operational Research* 197, 2 (2009), 685–692.

[25] Lamjed Ben Said, Slim Bechikh, and Khaled Ghédira. 2010. The r-dominance: a new dominance relation for interactive evolutionary multicriteria decision making. *IEEE transactions on Evolutionary Computation* 14, 5 (2010), 801–818.

[26] Kendall Taylor, Huong Ha, Minyi Li, Jeffrey Chan, and Xiaodong Li. 2021. Bayesian preference learning for interactive multi-objective optimisation. In *Proceedings of the Genetic and Evolutionary Computation Conference*. 466–475.

[27] Michał K Tomczyk and Miłosz Kadziński. 2020. On the elicitation of indirect preferences in interactive evolutionary multiple objective optimization. In *Proceedings of the 2020 genetic and evolutionary computation conference*. 569–577.

[28] Michał K Tomczyk and Miłosz Kadziński. 2021. Interactive evolutionary multiple objective optimization algorithm using a fast calculation of holistic acceptabilities. In *Proceedings of the Genetic and Evolutionary Computation Conference*. 476–484.

[29] Yash Vesikar, Kalyanmoy Deb, and Julian Blank. 2018. Reference point based NSGA-III for preferred solutions. In *2018 IEEE symposium series on computational intelligence (SSCI)*. IEEE, 1587–1594.

[30] Upali K Wickramasinghe, Robert Carrese, and Xiaodong Li. 2010. Designing airfoils using a reference point based evolutionary many-objective particle swarm optimization algorithm. In *IEEE congress on evolutionary computation*. IEEE, 1–8.

[31] Andrzej P Wierzbicki. 1980. The use of reference objectives in multiobjective optimization. In *Multiple criteria decision making theory and application*. Springer, 468–486.

[32] Deepanshu Yadav, Palaniappan Ramu, and Kalyanmoy Deb. 2023. Finding Robust Solutions for Many-Objective Optimization Using NSGA-III. In *2023 IEEE Congress on Evolutionary Computation (CEC)*. IEEE, 1–8.

[33] Deepanshu Yadav, Palaniappan Ramu, and Kalyanmoy Deb. 2023. Interpretable self-organizing map assisted interactive multi-criteria decision-making following Pareto-Race. *Applied Soft Computing* 149 (2023), 111032.

[34] Deepanshu Yadav, Palaniappan Ramu, and Kalyanmoy Deb. 2023. Multi-objective Robust Optimization and Decision-Making Using Evolutionary Algorithms. In *Proceedings of the Genetic and Evolutionary Computation Conference*. 786–794.

[35] Qingfu Zhang and Hui Li. 2007. MOEA/D: A multiobjective evolutionary algorithm based on decomposition. *IEEE Transactions on evolutionary computation* 11, 6 (2007), 712–731.

[36] Eckart Zitzler and Lothar Thiele. 1999. Multiobjective evolutionary algorithms: a comparative case study and the strength Pareto approach. *IEEE transactions on Evolutionary Computation* 3, 4 (1999), 257–271.

[37] Eckart Zitzler, Lothar Thiele, Marco Laumanns, Carlos M Fonseca, and Viviane Grunert Da Fonseca. 2003. Performance assessment of multiobjective optimizers: An analysis and review. *IEEE Transactions on evolutionary computation* 7, 2 (2003), 117–132.